THE JOURNAL OF PHYSICAL CHEMISTRY A

ARTICLE

pubs.acs.org/JPCA

Experimental Method to Measure the Effect of Charge on Bimolecular Collision Rates in Electrolyte Solutions

Barney L Bales,*[,†] Kathleen M. Cadman,[†] Mirna Peric,[†] Robert N. Schwartz,[‡] and Miroslav Peric[†]

[†]Department of Physics and Astronomy and The Center for Supramolecular Studies, California State University—Northridge, Northridge, California 91330, United States

[‡]Department of Electrical Engineering and Western Institute of Nanoelectronics, University of California—Los Angeles, Los Angeles, California 90095, United States

ABSTRACT: A stable, monoprotic nitroxide spin probe is utilized as a model to study molecular collisions in aqueous electrolyte solutions. The rate constants of bimolecular collisions, K_{col} for 2,2,5,5-tetramethylpyrrolidin-1-oxyl-3-carboxylic acid (CP) when it is uncharged (at low pH) and K_{col}^- when it is charged (CP^-; at high pH), are measured as functions of temperature and ionic strength. The ratio $f^* \equiv K_{col}^-/K_{col}$ is a direct measure of the effect of charge on the collision rate. Neglecting the small differences in size and diffusion coefficients of CP and CP^-, f^* is the fractional change in collision rate due to Coulomb repulsion which was treated theoretically in Debye's classic paper [*Trans. Electr. Chem. Soc.* **1942**, *82*, 265]. K_{col} and K_{col}^- are determined from EPR spectral changes due to spin−spin interactions which are dominated by Heisenberg spin exchange under the conditions of these experiments. Values of f^* vary linearly with values of $\kappa \cdot d$ in the range $0.4 < \kappa \cdot d < 1.8$, where κ and d are the inverse Debye screening length and the distance at closest approach, respectively. Values of d obtained in two independent ways, (1) from rotational correlation times measured by EPR and (2) by insisting that the experimental results be consistent with the Debye theory at infinite dilution, yield similar results. As the ionic strength is increased (κ increased), the screening effect reduces the effect of the Coulomb barrier more slowly than predicted by the Debye theory. While values of K_{col} and K_{col}^- vary substantially with T, approximately following the Stokes−Einstein−Smoluchowski equation, values of f^* depend only slightly on temperature at a given value of $\kappa \cdot d$, as is predicted by Debye's theory.

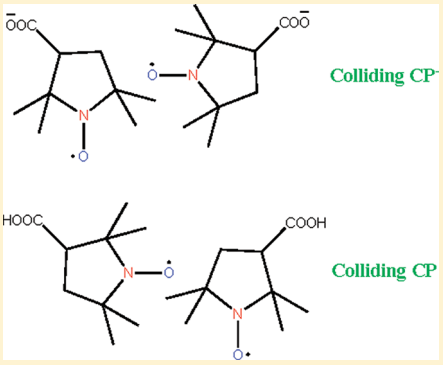

1. INTRODUCTION

Chemical reactions in solution depend on (A) the frequency of collision of the two reactants and (B) the efficacy of reaction once they are in contact. The former has been discussed in a vast literature, much of it building on the work of Smoluchowski[1] in the early 20th century. See ref 2 and the references therein. For the important problem of reaction rates in ionic solution between charged reactants, Debye derived an equation describing the effect of Coulomb attraction or repulsion on the bimolecular collision rate in ionic solutions.[2] To simplify the presentation, we outline below the results for univalent, like-charged reactants in solutions of univalent electrolytes. Debye's expression (eq 15 below) predicts the ratio of the collision rate constant of a particle when it is charged to when it is uncharged as follows:

$$f^* = \frac{K_{col}^-}{K_{col}} \tag{1}$$

Equation 1 suggests an interesting strategy to measure f^* employing the same molecule whose charge state is altered by varying the pH. In principle, any experimental approach could be fruitful provided the charges do not change the probability of reaction upon collision, that is, the efficacy of the reaction, item (B) is not altered. In practice, reactions dominated by item (A), diffusion controlled reactions, are more likely to be successful. Here, we detail a strategy of measuring K_{col} and K_{col}^- from the effect of concentration on the EPR spectra of nitroxide free radicals (nitroxides) whose charge state may be changed with pH. The "reaction" is the simplest known: the spin exchange of the two unpaired electrons of the two "reactants."[3−21]

When two free radicals collide, the orbitals of the two unpaired electrons may overlap leading to spin exchange with rate constant[4]

$$K_e = f_s \frac{1}{2} \frac{J^2\tau_c^2}{1 + J^2\tau_c^2} K_{col} \tag{2}$$

where J is equal to minus two times the exchange integral, τ_c is the mean time during a collision, and f_s an effective steric factor. Because of the short-range of the exchange integral, spin exchange is only effective when the colliding pair is in intimate contact.[4] The condition of strong exchange, that is, $J^2\tau_c^2 \gg 1$, has been found to hold for nitroxides except at very low values of the viscosity;[4,21] thus,

$$K_e = \frac{f_s}{2} K_{col} \tag{3}$$

Received: August 1, 2011
Revised: August 22, 2011
Published: August 25, 2011

The steric factor f_s for most small nitroxides is unity because any collision leads to spin exchange, even those that do not involve direct contact between the NO portions of the nitroxides.[4] Even if $f_s < 1$, it is not expected to depend on whether the nitroxide is charged or uncharged unless some change in conformation accompanies the change in charge state. This is because with the same geometry of the molecule the same atoms bearing unpaired spin density are available for contact.[4] Nevertheless, the Coulomb interaction is expected to change the molecular dynamics of the colliding pair and could affect the spin exchange efficiency because the rotational and translational motion of the partners during the interval between re-encounters might change f_s for the charged species. This point needs further theoretical development. To proceed, we assume that f_s is the same for the charged and uncharged species permitting an experimental value of f^* to be found from measurements of the spin exchange rate constants for the charged and uncharged species as follows:

$$f^* = \frac{K_e^-}{K_e} \tag{4}$$

Note that eq 4 minimizes systematic errors in the measurement of K_e and K_e^- because the same measurement procedures are used for both.

For our first effort, we studied 2,2,5,5-tetramethylpyrrolidin-1-oxyl-3-carboxylic acid (CP) in aqueous solution. By adding HCl or NaOH, we shift the following equilibrium to the left or right, respectively.

$$CP \leftrightarrow CP^- + H_3O^+ \tag{5}$$

In addition to providing a straightforward, reliable measurement of K_e^- and K_e, EPR offers three additional advantages. First, the value of the ^{14}N hyperfine spacing in the EPR spectrum reveals unequivocally whether the equilibrium eq 5 is predominantly to the right (charged) or the left (uncharged). Second, an independent measurement of the rotational correlation time allows an estimate of the hydrodynamic radius of the nitroxide. Third, a comparison between the rotational diffusion coefficients for CP and CP^- offers insight into the relative translational diffusion coefficient of the two states.[22]

2. THEORY

According to the theory of strong electrolytes,[2] the reciprocal thickness of the ionic layer (inverse screening length), κ, is defined by

$$\kappa^2 = \frac{e^2}{\varepsilon_0 \varepsilon_r kT} \sum n_i Z_i^2 \tag{6}$$

where e is the charge of an electron, ε_r the dielectric constant, T is the absolute temperature, and n_i is the number density of ions of type i with charge eZ_i. Evaluating the constants and changing units,

$$\kappa^2 = \frac{1265}{\varepsilon_r T} \sum C_i Z_i^2 \equiv K(T) \sum C_i Z_i^2 \tag{7}$$

where κ is given in $Å^{-1}$ with concentration of the ith ionic species, C_i, in mol L^{-1}. In these experiments involving only univalent species,

$$\sum C_i Z_i^2 = 2(C_{CP^-} + C_{NaCl} + C_{NaOH} + C_{HCl}) \equiv 2C_{total} \tag{8}$$

Utilizing data[23] for the temperature dependence of ε_r of water in the range 273−373 K, the temperature-dependent factor in eq 7 is given by $K(T) = 0.0648 - 1.38 \times 10^{-4}T + 3.43 \times 10^{-7}T^2$ $Å^{-2}$/mol L^{-1} to within the accuracy of the values of ε_r. One finds that κ varies modestly with T because ε_r decreases as T increases.

The equilibrium distance,[2]

$$l = \frac{Z_1 Z_2 e^2}{4\pi\varepsilon_0 \varepsilon_r kT} \tag{9}$$

is the distance between two ions where the Coulomb energy is equal to kT. For univalent ions in water,[23] $l = 8.552 - 1.823 \times 10^{-2}T + 4.537 \times 10^{-5}T^2$, in Å, which also varies modestly with T; see Figure 7.

In his classic paper,[2] Debye began with Smoluchowski's expression for the collision rate between uncharged particles and endeavored to calculate the effect of coulomb interactions as follows:

For simple Brownian motion, the number of collisions per second is given by[2,4]

$$\nu = 4\pi d D_M n \tag{10}$$

where d is the separation distance between the two particles at collision, D_M is the mutual diffusion coefficient, and n the particle (nitroxide) density. The Stokes−Einstein relation gives the particle translational diffusion coefficient, $D = D_M/2$ as

$$D = \frac{kT}{6\pi a \eta} \tag{11}$$

where a is the radius of the particle taken to be a sphere and η is the shear viscosity. Taking $d = 2a$, changing the concentration to mol L^{-1}, and combining eqs 10 and 11 yield the familiar form

$$\nu = K_D C \tag{12}$$

where C is the concentration of the colliding species; in this case, either C_{CP} or C_{CP^-} and the collision rate constant is given by

$$K_D = \frac{8RT}{3000\eta} \tag{13}$$

As is well-known, eq 13, the Stokes, Einstein, Smoluchowski equation (SES) is independent of the size of the diffusing particles.[2] Debye reasoned[2] that the collision rate ought to be altered by the Coulomb interaction between the charged particles so that the collision rate for CP^-, ν^-, would be

$$\nu^- = f^* 4\pi d D_M n \tag{14}$$

with

$$1/f^* = d \int_d^\infty \exp\left(\frac{U(r)}{kT}\right) \frac{dr}{r^2} \tag{15}$$

where $U(r)$ is the electrostatic interaction potential energy between the colliding pair separated by a distance r. Note that eqs 10 and 14 assume that D_M is the same for the charged and uncharged species. Freed and co-workers (see Appendix of ref 20 and references therein), proposed a form of eq 10 that takes into account other interaction potentials between radicals as well as the liquid structure via the pair-distribution function. Including the other interactions would result in a multiplicative factor in

eqs 10 and 14 involving an integral of the form eq 15. We assume that contributions to f^*, *other than the electrostatic interaction*, are the same. Therefore, in forming the ratio, eq 4, the effects of other potentials and liquid structure would cancel.

In the extreme dilute limit, using the Coulomb potential,

$$\frac{U(r)_{\mathrm{Coul}}}{kT} = l/r \tag{16}$$

the integral in eq 15 is easily solved to give

$$f^*_{\kappa=0} = \frac{l/d}{\exp(l/d) - 1} \tag{17}$$

As the ionic strength is increased, the Coulomb potential is no longer valid because of the shielding effects of the ionic cloud, and the challenge is to find a proper potential energy to use in eq 15.[2] Debye proposed,[2] for small values of κ and large r,

$$\frac{U(r)_{\mathrm{Debye}}}{kT} = \gamma \frac{l}{r} e^{-\kappa r} \tag{18}$$

that is, the Coulomb result, eq 16, multiplied by the factor $\gamma e^{-\kappa r}$, where

$$\gamma = \frac{e^{\kappa d/2}}{1 + \kappa d/2} \tag{19}$$

Equation 15 using eq 18 is of limited use in most experiments because it is only valid at concentrations below those of interest.

There is a huge literature seeking to extend the validity of Debye–Hückel (DH) theory[24] to higher concentrations to predict colligative properties of electrolyte solutions. Modern theories of electrolyte solutions are physically accurate[25] but difficult to apply. For a recent simplified treatment leading to mathematical expressions for the thermodynamic excess functions as well as an excellent summary of past work, see the recent work by Fraenkel.[25]

3. MATERIALS AND METHODS

The nitroxide 2,2,5,5-tetramethylpyrrolidin-1-oxyl-3-carboxylic acid (CP; 99%) and NaCl were purchased from Aldrich and used as received. All solutions were prepared in nanopure water by weight; the molar concentrations were corrected for the change in density due to the addition of salts.[26] NaOH (N/100 certified) was purchased from Fisher Scientific and HCl (ca. 32% solution in water) was purchased from Acros Organics. Preliminary measurements showed that CP is soluble in an excess of HCl to approximately 20 mM and CP^- in excess NaOH solutions to about 80 mM. A maximum concentration of the nitroxide was chosen to be 10 mM, a compromise between obtaining enough line broadening for accurate spectral parameter determination and gaining access to low values of κ. Six series of samples were prepared at nominal C_{CP} = 0.5, 2, 4, 6, 8, and 10 mM, each at a constant value of κ. The 10 mM solution was prepared with or without added NaCl and was diluted with a NaCl solution whose concentration matched the total concentration of ions in the 10 mM solution. Four series of CP^- with C_{NaOH}/C_{CP} = 2.4 were prepared and are denoted $CP^-(23)$, $CP^-(34)$, $CP^-(74)$, $CP^-(150)$, and $CP^-(600)$, where the number in the parentheses is the nominal value of C_{total} in mM; that is, one-half of the ionic strength, eq 8. Two series of CP, labeled CP(48) and CP(600), were similarly prepared with C_{HCl}/C_{CP} = 5. The series from which the titration curve, Figure 2 below, was derived was prepared by mixing the appropriate amounts of the following three stock solutions: (1) C_{CP} = 10 mM and C_{NaCl} = 48 mM; (2) C_{CP} = 10 mM and C_{HCl} = 48 mM; and (3) C_{CP} = 10 mM and C_{NaOH} = 48 mM. All of the calculations were made with the actual concentrations. These series ensure that the broadening varied linearly with C_{CP}, that is, that K_e and K_e^- are indeed constant.

The viscosity of the solutions were corrected for the presence of salts using the equations of ref 27. Most of the correction, which reaches a maximum of 7% at C_{NaCl} = 600 mM, is due to NaCl. Including all ions in the correction, using C_{total} rather than C_{NaCl} would only change the viscosity by a maximum of 0.6%.

The EPR spectra were measured with a Bruker 300 ESP X-band spectrometer and analyzed as detailed in recent papers.[28−32] The details describing how parameters are extracted from the experimental spectra by nonlinear least-squares fitting are summarized in Tables 1 and 2 of ref 32 and exhaustive descriptions of various factors in the analysis are given in the references found therein. The field sweep was calibrated with Bruker's NMR Gaussmeter operating in the 1-mG mode and was averaged over all of the runs with a particular sample. The accuracy of the magnetic field at the sample is estimated to be ±50 mG; however, the accuracy of the line widths and hyperfine coupling constants, being the difference of the magnetic fields is 1 − 2 mG. The reproducibility of these measurements may be judged from Figures 2 and 3, where results from five spectra are plotted separately. Each of the three EPR hyperfine lines is fit to a model of a Voigt absorption and a Lorentzian dispersion.[32] This fitting provides the interpolation between acquired points. The Voigt absorption of overall line width $\Delta H^0_{pp}(M_I)$ is then divided into a Lorentzian component due to spin relaxation of line width $\Delta H^L_{pp}(M_I)$ and a Gaussian component of line width $\Delta H^G_{pp}(M_I)$ due to inhomogeneous broadening, principally by unresolved hyperfine structure and field modulation.[33] The ^{14}N nuclear spin quantum number M_I = +1, 0, and −1 labels the low-, central, and high-field lines, respectively. As the nitroxide concentration is increased, the Lorentzian component of the line is broadened by spin exchange and dipole–dipole interactions:

$$B = \Delta H^L_{pp}(C_{CP}, M_I) - \Delta H^L_{pp}(0, M_I) = K_B C_{CP} \tag{20}$$

where B is the broadening and K_B is the broadening constant, both independent of M_I under the conditions of this work. In general, the broadening is the sum of those due to spin exchange and dipole–dipole interactions,[4,12,20,34]

$$B = B_e + B_{dip} \tag{21}$$

The broadening due to spin exchange, B_e, may be computed from the following:

$$B_e = \Omega(T) \cdot B \tag{22}$$

where $\Omega(T)$ is the fractional broadening due to spin exchange.[31]

The evaluation of $\Omega(T)$ is straightforward at high values of T/η, where it is of the order unity and becomes rather complex at low values, where $\Omega(T)$ approaches zero.[31] To avoid the problem of the separation of spin-exchange and dipole–dipole interactions, we performed these experiments at temperatures ≥298 K. In previous work,[31] we found that $\Omega(T) = 0.95 \pm 0.04$ in water at 283 K; above this temperature, $\Omega(T)$ is unity within

experimental uncertainty permitting us to neglect B_{dip}. See Figure 8a of ref 31 at T/η = 333 K/cP, corresponding to 298 K, the lowest temperature in this work.

From eq 20

$$K_B(M_I) = \frac{d\Delta H^L_{pp}(C_{CP}, M_I)}{dC_{CP}} \quad (23)$$

Because $K_e(M_I) = 3\sqrt{3}\gamma_e K_B(M_I)/4$ for $\Omega(T) = 1$,[4] where γ_e is the gyromagnetic ratio of the electron, eq 4 becomes the following:

$$f^* = \frac{K_B^-}{K_B} \quad (24)$$

At each temperature, three values of $K_B(M_I)$ and $K_B^-(M_I)$ are available from the slopes of $\Delta H^L_{pp}(C_{CP},M_I)$ versus C_{CP} for the three lines. With these three values from five spectra, yielding 15 values of $K_B(M_I)$ or $K_B^-(M_I)$, excellent statistics are available to compute mean values. Note that the evaluation of f^* from eq 24 does not depend on the Stokes−Einstein relation, eq 11, or any other assumed model of translational diffusion. The only requirement is that the diffusion coefficients of CP and CP^- be the same. The sole purpose in introducing eq 11 is to provide a rationale for the independent variable in Figure 4, below and to permit small corrections of the broadening constants for small differences in the viscosities of various solutions.

4. RESULTS AND DISCUSSION

4.1. Spectral Analysis. Figure 1 shows typical EPR spectra of CP^-(34) at 328 K. The fits overlay the experimental spectra; below each spectrum is the residual. Figure 1a is due to 0.0425 mM CP^-(34), where careful inspection of the spectrum and residual reveals lines due to hyperfine interaction with ^{13}C in natural abundance. Figure 1c, where the fit may be distinguished from the experimental spectrum by the solid line without noise, shows the central line of 1a on an expanded scale. Figure 1b displays the spectrum due to 10.1 mM CP^-(34) at a receiver gain one-fifth that of Figure 1a. The fits yield the absorption and the dispersion components of each line. The absorption components are not shown; the dispersion components are shown below the spectrum in Figure 1b. See ref 28 for examples of fits showing both the absorption and dispersion components. The central dispersion component is due to an improperly balanced microwave bridge and is used to correct the low- and high-field components (eq 5 of ref 32). These spectra and their fits may be compared with those in recent papers;[28−32,35] however, the inhomogeneous broadening due to unresolved hyperfine structure is much larger here. Our purpose in showing these spectra is to demonstrate that excellent fits are obtained even with large inhomogeneous broadening, allowing us to extract the Lorentzian components of the lines that are due to spin relaxation. The overall line width in Figure 1c is ΔH^0_{pp} = 1.266 ± 0.001 G, while the Lorentzian component has width ΔH^L_{pp} = 0.339 ± 0.002 G, where these are the mean values and standard deviations from five spectra taken one after another. Spectra from all samples at all temperatures, both CP and CP^-, are fit equally well. The difference in the resonance fields of the high- and low-field lines, $2A_{abs}$, is indicated in Figure 1b. Although the difference is imperceptible in Figure 1b, the difference in fields where the high- and low-field lines cross the baseline, $2A_{obs}$, is less than $2A_{abs}$; however, this difference is easily measured using spectral fitting.[31,35]

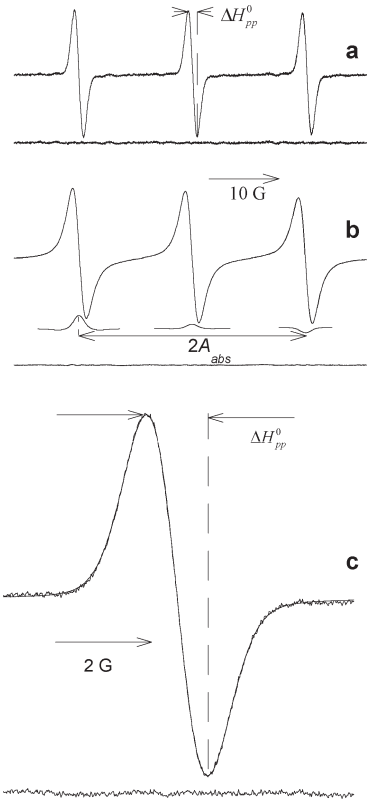

Figure 1. EPR spectra at 328 K of CP^-(34). (a) C_{CP^-} = 0.0425 mM and (b) C_{CP^-} = 10.1 mM. The nonlinear least-squares fits are indistinguishable from the spectra in (a) and (b); below each spectrum is the residual; that is, the difference in the spectra and the fits. Trace (c) shows the central line of (a) on an expanded scale; the fit is shown by the solid line without noise. Immediately below trace (b) is the dispersion component of the fit. The central dispersion component is due to an imbalanced microwave bridge and is used to correct the low- and high-field components, see text. The overall line width in (c) is ΔH^0_{pp} = 1.266 ± 0.001 G, while the Lorentzian component due to spin relaxation is only ΔH^L_{pp} = 0.339 ± 0.002 G, where these are the mean values and standard deviations from five spectra taken one after another. Inhomogeneous broadening dominates the line width; nevertheless, excellent fits are obtained.

Figure 2 shows the values of A_{abs} for C_{CP} = 0.1 mM (diamonds) and10.0 mM (circles) versus C_{NaOH}/C_{CP} or $-C_{HCl}/C_{CP}$ (plotted on the negative abscissa for clarity) at 298 K. Values from five spectra taken one after another, are plotted separately to illustrate the reproducibility. C_{total} = 58 mM for CP^- and 48 mM for CP. One sample, prepared with more NaCl so that C_{total} = 58 mM for CP, gave identical results for the uncharged species. The arrows (a) and (b) indicate the concentration ratios employed for all the other samples in this work. Note that the sample with no added base or acid is mostly charged at C_{CP} = 0.1 mM and mostly uncharged at10 mM. The reduction in A_{abs} at 10 mM is due to the well-known shifts of the hyperfine lines under the influence of spin exchange;[4,28−32,35] the reduction of A_{abs} being greater for CP than for CP^- because the spin exchange frequency is greater for the former. As Figure 2 shows, it is easy to maintain control over whether the spin probe is charged or uncharged by monitoring A_{abs}. Values of A_{abs} must be obtained from fits of the spectra such as those in Figure 1 and cannot be obtained by any simple measurement: however, as a practical matter, values of A_{obs} that may be obtained by simple measurements would provide an equally valid check on the charge state.

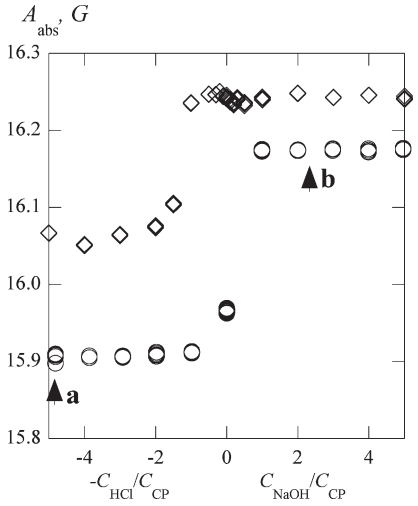

Figure 2. Hyperfine spacing, A_{abs}, for C_{CP} = 0.1 mM (diamonds) and 10.0 mM (circles) vs C_{NaOH}/C_{CP} or $-C_{HCl}/C_{CP}$ (plotted on the negative abscissa for clarity) at 298 K. Values from five spectra taken one after another are plotted separately to illustrate the reproducibility. For the 10.0 mM samples, NaCl is added to maintain C_{total} = 58 mM (screening length κ^{-1} = 12.5 Å). The arrows (a) and (b) indicate the concentration ratios employed for all the other samples in this work. Note that the sample with no added base or acid is mostly charged at C_{CP} = 0.1 mM and mostly uncharged at10.1 mM. The reduced values of A_{abs} for the more concentrated samples is due to the well-known line shifts due to spin exchange and this effect is larger for the uncharged species (added acid) than for the charged because the spin exchange frequency is larger for the former.

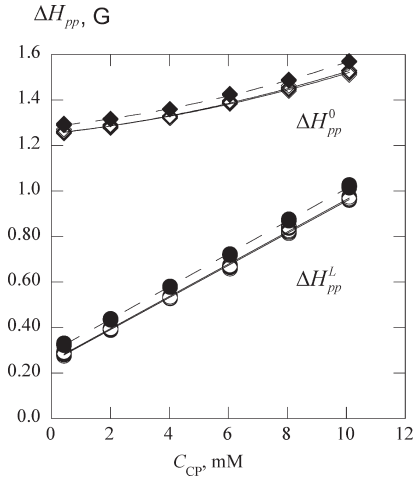

Figure 3. Overall line widths (diamonds) and the line widths of the Lorentzian component (circles) of the three lines of the $CP^-(34)$ series at 298 K. The results from five spectra are plotted separately to indicate the reproducibility; thus, each open symbol (low-field and central lines) is the superposition of 10 results and each closed (high-field line) of 5. The straight lines through the Lorentzian line widths are least-squares fits.

Figure 3 shows typical variations of ΔH^0_{pp} (diamonds) and ΔH^L_{pp} (circles) with nitroxide concentration for $CP^-(34)$ at 298 K. The line widths from the low-field and central line are plotted with the same open symbols, while those of the high-field line with solid symbols. Results from five spectra are plotted separately; thus, each open symbol is a superposition of 10 points

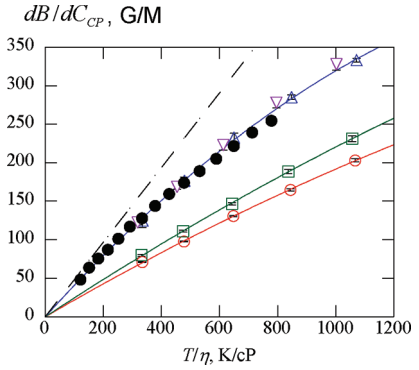

Figure 4. Broadening constants, eq 23, for $CP^-(34)$ (open circles), $CP^-(150)$ (squares), CP(48) (triangles), CP(600) (inverted triangles), and (uncharged) pDT taken from the literature[31] (closed circles). The curves through the data points are quadratics constrained to the origin. The dashed line is the SES, eq 13.

and each solid symbol of 5. The straight lines (solid for M_I = +1 and 0 and dashed for M_I = −1) through the values of ΔH^L_{pp} are least-squares fits with coefficients of correlation $r > 0.999$. Averaging over the three lines, yields a mean value and standard deviation of $K_B = 70.9 \pm 0.6$ G/M. The curves through the values of ΔH^0_{pp} are quadratics to guide the eye; a linear fit falls outside of the uncertainty.

Figure 3 re-emphasizes[36] the importance of extracting the correct Lorentzian component from the observed resonance line. Values of ΔH^0_{pp} are as much as a factor of 4.7 times too large and values of K_B determined by linear fits to ΔH^0_{pp} are too small by a factor of 2.5. Values of ΔH^L_{pp} vary linearly with nitroxide concentration with a coefficient of correlation $r > 0.999$ or better for all sample series at all temperatures; thus, K_B and $K_{\bar{B}}$ are constant at each temperature for all series.

In Figure 4 representative variations of K_B with T/η for two of the charged series, $CP^-(34)$ and $CP^-(150)$, and the two uncharged series, CP(48), and CP(600) are shown. The solid lines are least-squares fit ($r > 0.999$) of the results for $CP^-(34)$, $CP^-(150)$, and CP(48) to quadratics constrained to the origin. The fits to the other two series not shown are equally as good. The solid circles are data taken from the literature[31] for perdeuterated 2,2,6,6-tetramethyl-4-oxopiperidine-1-oxyl (pDT) in water showing that the uncharged CP collides at the same rate as the (uncharged) pDT. The excellent fits of the data to quadratic forms allow us to interpolate the data to common values of T/η (taken to be pure water) so that the ratios in eq 24 may be formed at the same temperature.

Line shifts are another independent source of information about molecular collisions.[4,28−32,35] In particular, information about re-encounters of the same colliding molecules while occupying the same "cage" is a topic of current interest.[30,34,37] These results will be reported elsewhere together with other systems.

4.2. Fixing the Distance of Closest Approach. An advantage of EPR is that measurement of the rotational correlation time, τ_{rot},[38,39] yields an independent estimate of the hydrodynamic radius of the spin probe, a, as follows:[40]

$$\tau_{rot} = \frac{4\pi}{3k} a^3 \cdot \frac{\eta}{T} \qquad (25)$$

which predicts a straight line passing through the origin when τ_{rot} is plotted against η/T. Figure 5 shows a representative plot (for

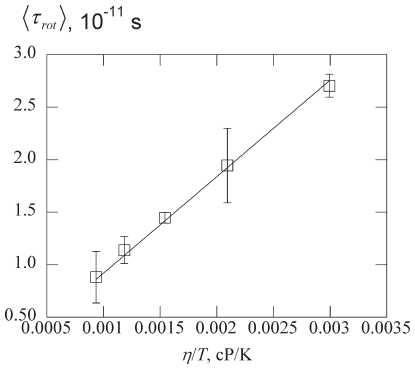

Figure 5. Rotational correlation time of 0.0425 mM CP^-(34). The straight line is a linear fit to eq 25 weighting each datum by its inverse variance[41] yielding a hydrodynamic radius of a = 3.13 ± 0.06 Å. The error bars are standard deviations of values derived from 5 spectra. The average over all samples yields a = 3.23 ± 0.06 Å.

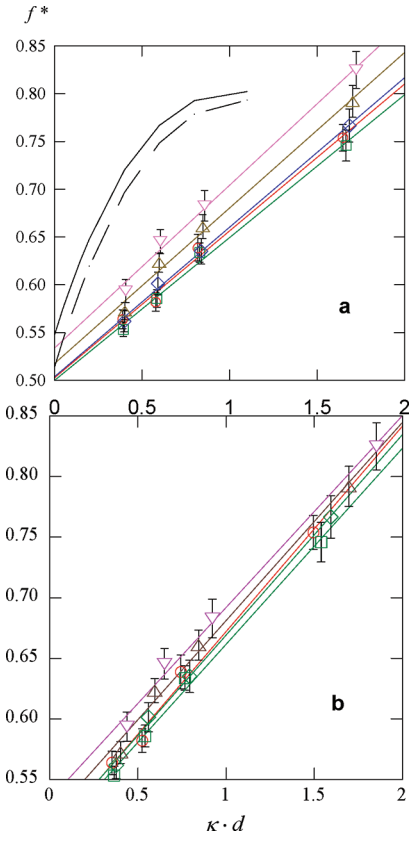

Figure 6. Ratios of the collision frequencies of CP^- to CP at 298 (circles), 313 (squares), 328 (diamonds), 343 (triangles), and 358 K (inverted triangles) versus $\kappa \cdot d$ with the distance of closest approach d fixed by (a) $d = 2a$, where a = 3.23 Å, determined from rotational correlation times and (b) fixed to the values given in Figure 7 by setting the intercept at each temperature to that predicted by Debye's theory[2] in the limit of infinite dilution, eq 17. The straight lines are linear fits to the data and the curved lines are Debye's theory[2] at 298 (solid) and 358 K (dashed).

$CP(34)^-$) showing the mean and standard deviation derived from 5 spectra. The straight line is a linear least-squares fit constrained to the origin weighting each datum by its inverse variance.[41] From the resulting slope of the fit, a = 3.13 ± 0.06 Å

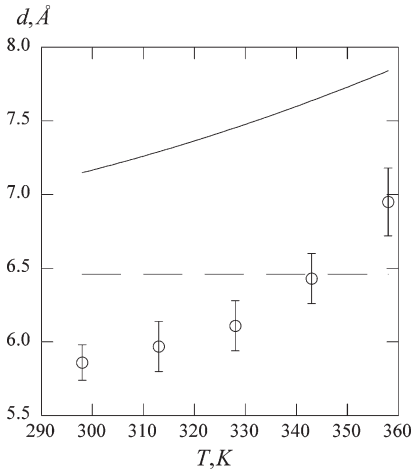

Figure 7. Values of the distance of closest approach determined by setting the intercept of the straight lines in Figure 6 to the value given in eq 17. The error bars are propagated from the errors in the values of the intercepts. The dashed line is the value fixed by independent rotational correlation time measurements. The solid line gives values of l, eq 9.

for $CP(34)^-$. Averaging over all series, the mean value is given by a = 3.27 ± 0.07 Å for CP and a = 3.15 ± 0.03 Å for CP^-. Averaging all seven series yields a = 3.23 ± 0.06 Å, which we adopt for the calculations below. Compare this with the value a = 3.2 Å reported[20] for pDT. The near coincidence in the values of a for CP and CP^- supports the assumption that D_M is similar for the two. To proceed, we assume that the hydrodynamic radius for rotation is the same as that for translation and further assume that the distance of closest approach, $d = 2a$.

4.3. Variation of *f with Temperature and Screening Length.** Figure 6 shows the central results of this work. With d fixed, we may plot values of f^* versus $\kappa \cdot d$ without any adjustable parameters. These data are shown in Figure 6a at 298 (circles), 313 (squares), 323 (diamonds), 343 (open triangles), and 358 K (inverted triangles) together with the predictions of the Debye theory at 298 (solid line) and 358 K (dashed line). The Debye results were found by numerical integration of eq 15 employing eq 18. These results are presented up to $\kappa \cdot d$ = 1; however, the theory is only valid near the origin. The straight lines through the data points are least-squares fits to guide the eye. The most striking feature of Figure 6 is the minor dependence on the temperature for both the theory and the experiment results. Clearly, at low ionic strength, the extrapolated experimental results are comparable to the theoretic prediction. Because there are no adjustable parameters in Figure 6a, the method of obtaining f^* from EPR using eq 24 appears to be valid as are the assumptions that $d = 2a$, and that a obtained from rotational correlation times serves to fix the distance of closest approach.

If we extrapolate the experimental results to the origin and insist that they be equal to the theoretical prediction, eq 17, then experimental values of d may be found. Carrying this out and replotting the data in Figure 6a results in Figure 6b, showing that experimental results are independent of the temperature provided that d is adjusted. The similarity of Figure 6a and b shows that the adjusted values of d are not very different from those fixed by independent measurements of the rotational correlation time. The adjusted values of d are shown in Figure 7 together with values of l. The error bars show the uncertainty in d due to the uncertainty in the extrapolated values in Figure 6a.

The design of the present experiment is as well as we can do for values of $\kappa \cdot d > 0.4$. Uncertainties due to the concentration (both are prepared from the same stock solution) are compensated by forming the ratio of the collision rates in the charged and uncharged species. Uncertainities in the temperature are unimportant given the near temperature-independence of the results in Figure 6. If there are small systematic errors in the extraction of values of ΔH_{pp}^{L} from the least-squares fits, these are expected to be very similar because the line widths and shapes are similar. Higher concentrations are of practical interest because most chemistry is preformed at concentrations too high to apply Debye's theory. The present design cannot yield results at low values of $\kappa \cdot d$ because to get reliable results, one needs to use at least 10 mM of CP^-, which requires 22 mM NaOH to ensure that the species is charged. Therefore, keeping in mind that the Debye theory is only valid for small values of $\kappa \cdot d$, a direct comparison is not possible. Nevertheless, it is clear that extrapolated values of f^* are consistent with the theory.

The fact that the broadening rate constants for the uncharged pDT and the uncharged CP are the same (Figure 4) is encouraging. This means that meaningful results may be obtained from a charged small nitroxide using the results from Figure 4 for the uncharged species. Thus, salts of similar small nitroxides rather than their acids could be used which would obviate the need for the added base or acid, ultimately allowing us to reduce the concentration by more than a factor of 3. There is another implication of the similarity of the broadening constants for the two uncharged nitroxides. One (pDT) is derived from a perdeuterated probe resulting in small inhomogeneous broadening due to unresolved hyperfine structure and the other (CP) is severely broadened inhomogeneously. Thus, it appears that these experiments may be performed with less costly probes without deuteration provided that the spectra are fit to a Voigt line shape.

4.4. Modifications to Debye Theory. The reduction of the coulomb barrier provided by the shielding effect of the ions proceeds at a slower function of κ than predicted by Debye's theory which is only valid for large values of r and low concentrations, neither of which conditions is fulfilled. In any discussion of collisions, one must consider values of $r \approx d$. One reason to expect a larger repulsion in the real system as opposed to eq 18 is because the theory assumes that the shielding effect is in full force even at short distances where the shielding is expected to be smaller because that portion of the ionic cloud lying at distances larger than $r \approx d$ is not effective in reducing the electric field. It is beyond the scope of this initial work to seek a detailed rationalization of the results in Figure 6, which would require finding a scientifically sound function $U(r)$ that would agree with the experimental results. Our main goal in this work is to provide a reliable experimental basis to compare with theory; nevertheless, it seems useful to estimate the effect of reducing the screening effect at close distances. We also suggest a simple way to include high electrolyte concentrations into an alternate potential to that in eq 18.

In the original DH theory,[24] where ionic sizes are ignored, κ emerges as the inverse mean radius of the ionic atmosphere.[42] Including an "apparent" diameter, a', in the theory shows that $\kappa^* = \kappa/(1 + \kappa a')$ plays that same role. See, for example, the development leading to eq 3-5-5 of ref 42 for details. This simple extension of the original DH theory was meant to improve the predictions of the theory in which the parameter a was supposed to be the average distance to which ions can approach one another, both positive and negative. If we continue to regard the ions of the electrolytes as point charges and identify $a' = d$ as the distance to which the colliding CP^- ions approach, then a natural extension to eq 8 is as follows:

$$\frac{U(r)}{kT} = \gamma^* \frac{l}{r} e^{-\kappa^* r} \tag{26}$$

where

$$\gamma^* = \frac{e^{\kappa^* d/2}}{1 + \kappa^* d/2} \tag{27}$$

Taking the inverse screening length to be equal to κ is only valid at very low concentrations and loses meaning when $\kappa \cdot d$ approaches unity because the ionic cloud does not extend beyond the surface of the ion; however, taking $\kappa/(1 + \kappa d)$ to be the inverse screening length avoids this difficulty. Equation 26 becomes identical to eq 18 in the limit in which the theory is valid.

Turning to screening at close distances, Kirkwood[43] suggested that all screening effects including fluctuations be ignored when $r < r_0$, where r_0 was unspecified but ought to be less than $1/\kappa$. To estimate the impact of removing the screening effect at short distances, we have "turned off" the screening effect in two ways. First, we maintain the full Coulomb potential for distances less than r_0; that is,

$$\frac{U(r)}{kT} = \frac{l}{r} \tag{28}$$

for $r = r_0$ to $r = d$ and equal to eq 18 for $r \geq r_0$. Second, we change the factor $\gamma e^{-\kappa r}$ in eq 18 to unity linearly from $r = r_0$ to $r = d$. Thus, for $d \leq r \leq r_0$, the potential becomes

$$\frac{U(r)}{kT} = \frac{l}{r} \frac{1}{r_0 - d}[(r_0 - r) + (r - d)\gamma \exp(-\kappa r_0)] \tag{29}$$

and equal to eq 18 for $r \geq r_0$. Rather than treat r_0 as an adjustable parameter, we estimate the effect of eqs 28 and 29 by taking $r_0 = 1/\kappa$.

The results of these modifications are shown in Figure 8 for 343 K showing eq 15 employing eq 18 (solid line), eq 29 (long dashes), eq 26 (intermediate dashes), and eq 28 (shortest

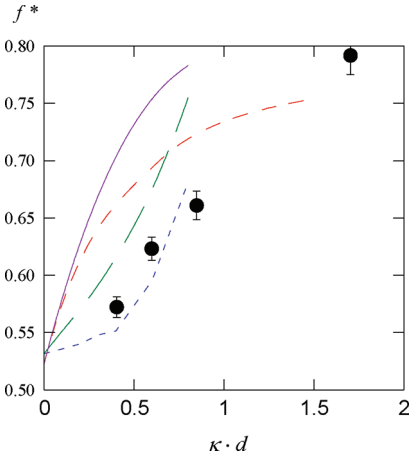

Figure 8. Results of modifications of the standard theory, eq 18 (solid line), at 343 K. Results of eq 15 employing eq 29 (long dashes), eq 26 (intermediate dashes), and eq 28 (shortest dashes). The solid circles are the experimental results for 343 K. Reducing the screening effect at close distances improves the predictions at low values of $\kappa \cdot d$ while using a modified $\kappa^* = \kappa/(1 + \kappa \cdot d)$ improves them at higher values.

dashes). The solid circles are the experimental results for 343 K. All three modifications tend to lower the predicted values of f^* as expected. The two modifications reducing the effect of screening at close distances (long and short dashes) improve the predictions at low values of $\kappa \cdot d$ and the use of the alternate screening length $1/\kappa^*$ improves the predictions at larger values.

5. FUTURE WORK

Modeling of collisions of molecules using nitroxide free radicals appears to be a promising technique. Future work could focus on the effect of charge on collisions in complex fluids liquids, explore the effects of dielectric constant, and the dependence of collision rate in the presence of electrolyes of different valences. A particularly interesting focus might be on collision rates of charged molecules in ionic solvents where the screening lengths would be very short. We have been careful in this first experiment to vary the concentration of CP to ensure that the broadening constants are indeed constant, because with large inhomogeneous contributions to the line widths, there could be potential problems. It appears that the methods are accurate even with large inhomogeneous contributions to the line width; thus, much simpler designs in which just two concentrations, on the order of 0.1 and 10 mM, respectively, will give reliable results. We have already pointed out the advantages to using nitroxide salts rather than acids and in using values of the broadening constants for uncharged, small nitroxide from Figure 4. This work was carried out above 298 K to keep the analysis simple and concentrate on the method. The same approach is available for lower temperature and higher viscosity solvents and mixtures; however, the more complicated methods detailed in ref 31 would be required to extract $K_e = \Omega \cdot K_B$ and $K_e^- = \Omega^- \cdot K_B^-$. It appears that future exploratory work can concentrate on one temperature, investigating other experimental parameters.

6. CONCLUSIONS

EPR of nitroxide radicals whose charge state may be altered with pH is demonstrated to afford measurements of $f^* = \nu^-/\nu$, where ν^- and ν are the bimolecular collision rates of the charged or uncharged species, respectively. Forming the ratios of the broadening constants of CP^- to CP yield experimental values of f^* as functions of T and κ. Comparing these with those predicted theoretically by eq 15, employing eq 18, demonstrates that both experiment and theory show minor temperature dependence and that the reduction of the Coulomb barrier provided by the ionic cloud is a weaker function of κ than predicted. Simple modifications to the theoretical prediction can bring experiment and theory into reasonable agreement.

AUTHOR INFORMATION

Corresponding Author

*E-mail: barney.bales@csun.edu.

REFERENCES

(1) Smoluchowski, M. V. *Z. Phys. Chem.* **1917**, *92*, 129–168.
(2) Debye, P. *Trans. Electrochem. Soc.* **1942**, *82*, 265–272.
(3) Kivelson, D. *J. Chem. Phys.* **1960**, 33, 1094–1106.
(4) Molin, Y. N.; Salikhov, K. M.; Zamaraev, K. I. *Spin Exchange. Principles and Applications in Chemistry and Biology*; Springer-Verlag: New York, 1980; Vol. 8.
(5) Freed, J. H. *J. Chem. Phys.* **1966**, *45*, 3452–3453.
(6) Jones, M. T. *J. Chem. Phys.* **1963**, *38*, 2892–2895.
(7) Salikhov, K. M.; Doctorov, A. B.; Molin, Y. N.; Zamaraev, K. I. *J. Magn. Reson.* **1971**, *5*, 189–205.
(8) Currin, J. D. *Phys. Rev.* **1962**, *126*, 1995–2001.
(9) Ayant, Y.; Besson, R.; Salvi, A. *J. Phys. (Paris)* **1975**, *36*, 571–580.
(10) Johnson, C. S., Jr. *Mol. Phys.* **1967**, *12*, 25–31.
(11) Stillman, A. E.; Schwartz, R. N. *J. Magn. Reson.* **1976**, *22*, 269–277.
(12) Berner, B.; Kivelson, D. *J. Phys. Chem.* **1979**, *83*, 1406–1412.
(13) Kovarskii, A. L.; Wasserman, A. M.; Buchachenko, A. L. *J. Magn. Reson.* **1972**, *7*, 225–237.
(14) Eastman, M. P.; Kooser, R. G.; Das, M. R.; Freed, J. H. *J. Chem. Phys.* **1969**, *51*, 2690–2709.
(15) Eastman, M. P.; Bruno, G. V.; Freed, J. H. *J. Chem. Phys.* **1970**, *52*, 2511–2522.
(16) King, M. D.; Sachse, J. H.; Marsh, D. *J. Magn. Reson.* **1987**, *72*, 257–267.
(17) Sachse, J. H.; King, M. D.; Marsh, D. *J. Magn. Reson.* **1987**, *71*, 385–404.
(18) Martini, G.; Bindi, M. *J. Colloid Interface Sci.* **1985**, *108*, 133–139.
(19) Miller, T. A.; Adams, R. N.; Richards, P. M. *J. Chem. Phys.* **1966**, *44*, 4022–4024.
(20) Nayeem, A.; Rananavare, S. B.; Sastry, V. S. S.; Freed, J. H. *J. Chem. Phys.* **1989**, *91*, 6887–6905.
(21) Plachy, W.; Kivelson, D. *J. Chem. Phys.* **1967**, *47*, 3312–3318.
(22) Buchachenko, A. L.; Wasserman, A. M.; Kovarskii, A. L. *Int. J. Chem. Kinet.* **1969**, *1*, 361–370.
(23) *CRC Handbook of Chemistry and Phyisics*, 73rd ed.; CRC Press: Boca Raton, FL, 1992.
(24) Debye, P.; Hückel, E. *Z. Phys.* **1923**, *24*, 185–206.
(25) Fraenkel, D. *Mol. Phys.* **2010**, *108*, 1435–1466.
(26) *Handbook of Chemistry and Physics*, 31st ed.; Chemical Rubber Publishing: Cleveland, OH, 1949.
(27) Kestin, J.; Khalifa, H. E.; Abe, Y.; Grimes, C. E.; Sookiazian, H.; Wakeham, W. A. *J. Chem. Eng. Data* **1978**, *23*, 328–336.
(28) Bales, B. L.; Peric, M. *J. Phys. Chem. A* **2002**, *106*, 4846–4854.
(29) Bales, B. L.; Peric, M.; Dragutan, I. *J. Phys. Chem. A* **2003**, *107*, 9086–9098.
(30) Bales, B. L.; Meyer, M.; Smith, S.; Peric, M. *J. Phys. Chem A* **2008**, *112*, 2177–2181.
(31) Bales, B. L.; Meyer, M.; Smith, S.; Peric, M. *J. Phys. Chem A* **2009**, *113*, 4930–4940.
(32) Bales, B. L.; Harris, F. L.; Peric, M.; Peric, M. *J. Phys. Chem A* **2009**, *113*, 9295–9303.
(33) Bales, B. L.; Peric, M.; Lamy-Freund, M. T. *J. Magn. Reson.* **1998**, *132*, 279–286.
(34) Salikhov, K. M. *Appl. Magn. Reson.* **2010**, *38*, 237–256.
(35) Bales, B. L.; Peric, M. *J. Phys. Chem. B* **1997**, *101*, 8707–8716.
(36) Bales, B. L. Inhomogeneously Broadened Spin-Label Spectra. In *Biological Magnetic Resonance*; Berliner, L. J., Reuben, J., Eds.; Plenum Publishing Corporation: New York, 1989; Vol. 8, pp 77−130.
(37) Salikhov, K. M. *J. Magn. Reson.* **1985**, *63*, 271–279.
(38) Marsh, D. Experimental Methods in Spin-Label Spectral Analysis. In *Spin Labeling. Theory and Applications*; Plenum Publishing Corporation: New York, 1989; Vol. 8; pp 255−303.
(39) Schreier, S.; Polnaszek, C. F.; Smith, I. C. P. *Biochim. Biophys. Acta* **1978**, *515*, 395–436.
(40) Jones, L. L.; Schwartz, R. N. *Mol. Phys.* **1981**, *43*, 527–555.
(41) Bevington, P. R. *Data Reduction and Error Analysis for the Physical Sciences*; McGraw-Hill: New York, 1969.
(42) Harned, H. S.; Owen, B. B. *The Physical Chemistry of Electrolytic Solutions*, 3rd ed.; Reinhold: New York, 1958.
(43) Kirkwood, J. G. *J. Chem. Phys.* **1934**, *2*, 767–781.